Substitution effects on bipolarons in alkoxy derivatives of poly(1,4-phenylene-vinylene)

K. F. Voss, C. M. Foster, L. Smilowitz, D. Mihailović, S. Askari, G. Srdanov, Z. Ni, S. Shi, A. J. Heeger, and F. Wudl
Institute for Polymers and Organic Solids, University of California at Santa Barbara, Santa Barbara, California 93106
(Received 10 August 1990)

We have studied the vibrational and electronic structure and the elementary charged excitations of poly(1,4-phenylene-vinylene) and a series of its (2,5-alkoxy) derivatives including poly(2,5-methoxy-PV), poly(2,5-hexoxy-PV), poly(2,5-octoxy-PV), and poly[2-methoxy,5-(2′ethyl-hexoxy)-PV] by absorption, photoinduced (PI) absorption, and doping-induced (DI) absorption. For the pristine materials, we observe that the band gap decreases by as much as ~ 0.3 eV with the introduction of alkoxy side chains. We assign the observed ir-active phonons to specific structural vibrations. Upon either PI or DI carrier injection, we observe a series of infrared-active vibrational (IRAV) modes and two subgap electronic absorptions that we associate with the formation of bipolarons. Assignment of the IRAV modes indicates that the charged bipolarons couple strongly to lattice modes of the polymer backbone, and the measured IRAV mode frequencies indicate that the pinning strength of bipolarons in a given system decreases as the length of the side chain increases. In addition, from the energy of the two subgap electronic absorptions, we determine that the confinement parameter γ increases, the Coulomb interaction energy U_b remains unchanged, and the Coulomb binding energy E_b decreases with sidechain length.

I. INTRODUCTION

Interest in conducting polymers originated from the discovery that their electrical conductivity can be varied from an initially insulating state to a highly conducting state through either p-type or n-type doping. Conduction in these systems exhibits quasi-one-dimensional behavior in which the charged excitations of the π-electron band strongly couple to the polymer backbone. These nonlinear excitations are in the form of confined soliton pairs (polarons and bipolarons) in systems which have a nondegenerate ground state.[1,2]

A direct consequence of the formation of self-localized charged excitations in quasi-one-dimensional conjugated polymers is the development of infrared-active vibrational (IRAV) modes with associated electronic state(s) in the π-π^* energy gap. Due to the electron-phonon interaction, a charged excitation in the system causes a localized distortion of the π-electron charge density, which distorts the lattice in the vicinity of the carrier. This structural distortion breaks the local symmetry of the lattice, splitting off localized phonon modes (IRAV's) which represent the normal modes of the structural distortion. Each mode corresponds to one of the Raman-active optical-phonon bands of the polymer and appears with enhanced infrared oscillator strength due to coupling to the π-electron system. As a result of this distortion, the π-electron system forms self-localized electronic states in the gap at the expense of the π-π^* transition, giving rise to new subgap absorptions. Thus, the IRAV modes and the subgap electronic absorptions provide a "fingerprint" of the charged excitations of the polymer system.

The effects of carrier injection on the structural and electronic properties of conjugated polymers can be studied by using either chemical doping or photoexcitation at energies greater than the π-π^* interband transition. The unique advantage of photoexcitation is that the nonlinear charged excitations of the polymer are created via the decay of photogenerated electron-hole pairs and can be studied without the addition of disorder due to the presence of dopant counter ions in the polymer matrix. As a result, the spectral fingerprints produced by photoexcitation are not marred by the effects of dopant counter ions and are unambiguously assigned to charged excitations. Moreover, photoexcitation experiments have become particularly relevant since photoinduced shifts of oscillator strength have been proposed as a mechanism for the subpicosecond nonlinear optical properties and $\chi^{(3)}$ response observed in conjugated polymers.[3]

The synthesis of high molecular weight films of poly(phenylene-vinylene) (PPV) through a precursor polymer route[4] offers the opportunity for experimental study of high-quality samples of these conjugated polymers.[5–9]

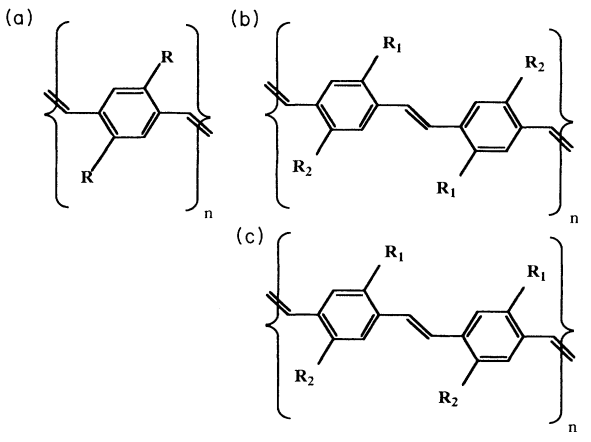

FIG. 1. The chemical structure of PPV and its alkoxy derivatives: (a) PPV: R = H, DMO: R = O-CH_3, DHO: R = O-$(CH_2)_5$-CH_3, DOO: R = O-$(CH_2)_7$-CH_3; (b) and (c) MEH: R_1=O-CH_3, R_2 = O-CH[$(CH_2)_5$-CH_2](CH_3); (b) is the centrosymmetric *head-to-tail* structure and (c) the noncentrosymmetric *head-to-tail* structure.

Although fully converted PPV has excellent mechanical properties, the material is intractable and further processing impossible. Derivatives of PPV have been achieved via the introduction of long chain alkoxy side groups attached onto the phenylene ring at the 2,5-carbons[10–12] (see Fig. 1), increasing both their solubility and environmental stability. Thus, the unique structure of the soluble PPV derivatives yields an attractive combination of electronic and mechanical properties and are promising materials from an engineering standpoint.

Established theoretical treatments assume that the addition of side chains to the polymer backbone will have no direct effect upon the π-electron system of a conjugated polymer,[1] as the conjugated double bond character of the backbone will be affected only in second order. However, the relative energy of the electronic bands can change depending on the electronegativity of the substituent group. In addition, the introduction of long side chains should increase the interchain distance, thereby decreasing the electronic coupling between chains. This paper investigates this assumption quantitatively by comparing the excitation spectra of a class of polymers with different substituents.

II. EXPERIMENTAL

A. Materials synthesis and doping

The synthesis routes of the polymers PPV,[13] poly(2,5-methoxy-PV) (DMO),[14,15] poly(2,5-hexoxy-PV) (DHO),[10] poly(2,5-octoxy-PV) (DOO),[10] and of poly[2-methoxy,5-(2′ ethyl-hexoxy-PV)] (MEH) (Ref. 11) are published elsewhere. Films of the PPV precursor were cast under nitrogen atmosphere from aqueous solution onto AgBr or sapphire substrates; films of the DMO precursor were cast in air from MeOH solution onto KBr substrates. Both were converted under dynamic vacuum (10^{-6} Torr) at 300 °C for 5 h. The MEH, DHO, and DOO precursor polymers were converted in solution, precipitated into powders, and redissolved in hot ($T \approx 100$ °C) organic solvents. Films were cast onto KBr substrates in air from either trichlorobenzene (DHO and DOO) or *m*-xylene (MEH) solutions. The samples were stored in a nitrogen dry-box (PPV) or a desiccator (DMO, MEH, DHO, and DOO). Following the photoinduced experiments, the DMO, MEH, DHO, and DOO samples were doped by immersion into 2% $FeCl_3$ solution for 20–30 sec under nitrogen atmosphere. PPV samples were found not to dope with $FeCl_3$; consequently, samples were doped by exposure to iodine vapor for 72 h or by immersion in concentrated H_2SO_4 for 10 sec.

B. Excitation spectroscopy

The ir spectra were taken with an IBM IR/98 Fourier-transform infrared (FTIR) spectrometer under dynamic vacuum at $\sim$ 80 K. For the ir photoexcitation experiment, the FTIR was modified to allow a laser beam coincident on the sample with the infrared probe beam as described by Blanchet *et al.*[16] Photoexcitations were created at $\sim$ 10 K by a cw Ar^+ laser utilizing the 514-nm line with an intensity of $\sim$ 40 mW/cm^2. Light and dark interferograms were taken alternately for 8 scans, and long time signal averaging of data ($\sim$ 6000 scans) was used to achieve a satisfactory signal-to-noise ratio. The ratio of these signal-averaged spectra directly yielded the change in the transmission, $\Delta T/T$, of the sample as a result of the photoexcitations caused by the laser. The $\Delta T/T$ induced upon doping was computed by subtracting the spectra of the doped samples from spectra recorded prior to doping.

The optical absorption spectra were measured with a Perkin-Elmer $\lambda 9$. The photoinduced absorption measurements were made using a two-beam technique, while the direct intensity of the broad band probe beam was measured in a standard transmission setup. A tungsten-halogen white light source (Newport model 780) illuminated the sample. The transmission as a function of wavelength was measured with a monochrometer (McPhearson model EU-700) and a two-color Si/PbS detector. The incident light was chopped and the transmission signal detected with a lock-in amplifier in order to enhance the signal-to-noise ratio. The photoexcited carriers were made by pumping across the gap with an Ar^+ laser using the following energy (nm) and power (mW) for each system: 458 and 90 (PPV), 514 and 300 (DMO), 514 and 140 (MEH), 514 and 60 (DHO), and 488 and 120 (DOO). The photoinduced absorption was measured by chopping the pump beam and locking in to the modulated component of the transmitted probe beam. From the ratio $\Delta T/T$, the change in the absorption upon opti-

cal pumping was obtained. Strong luminescence signals in all materials hampered observation of photoinduced bleaching above the gap.

III. RESULTS

A. Infrared and optical absorption

Figure 2 presents the mid-infrared phonon modes of PPV and its alkoxy derivatives in the ir region from 400 to 4500 cm^{-1}. The spectra have been scaled to the C-C semicircle ring stretch mode at $\sim$ 1510 cm^{-1}. In the case of PPV, calculations have shown that mode assignments in the corresponding monomer compare well with those of the polymer,[17] as modes which depend upon the degree of polymerization (e.g., simultaneous vibrations of the rings and vinyl bonds) and can shift considerably with conjugation length mostly occur at frequencies below 700 cm^{-1}. In Table I we list the phonon frequencies, relative intensities, and preliminary assignments to specific structural vibrations of the observed ir-active modes.[18] It is clear that the optical phonons in the materials exhibit good group frequencies. The observed phonons of PPV agree with data published by other groups.[5,6] With the addition of alkoxy side groups, modes due to methoxy, methyl, and methylene groups appear at frequencies similar to those found in small molecules.[18] We note that benzene-moiety-associated modes are mostly insensitive to the addition of the alkoxy side groups. In the region from 1600 to 2800 cm^{-1}, we observe a well-defined overtone and combination band spectrum. We detected no carbonyl contamination in any of our samples during the experiments, is as evidenced by the absence of the C=O stretch vibration at $\sim$ 1690 cm^{-1}.

Of particular interest is the *trans*-vinylene C=C stretch mode at $\sim$ 1640 cm^{-1}, weakly observed in PPV, DMO, DHO, and DOO, while pronounced in MEH. In systems which have a center of inversion, this mode is centrosymmetric and strictly Raman active. The weak intensity of these modes in PPV, DMO, DHO, and DOO implies weak symmetry breaking due to disorder, which we attribute to such effects as crosslinking, chain-end effects, and, in the case of the alkoxy derivatives, sterically less preferable head-to-head configurations. For MEH, the in-

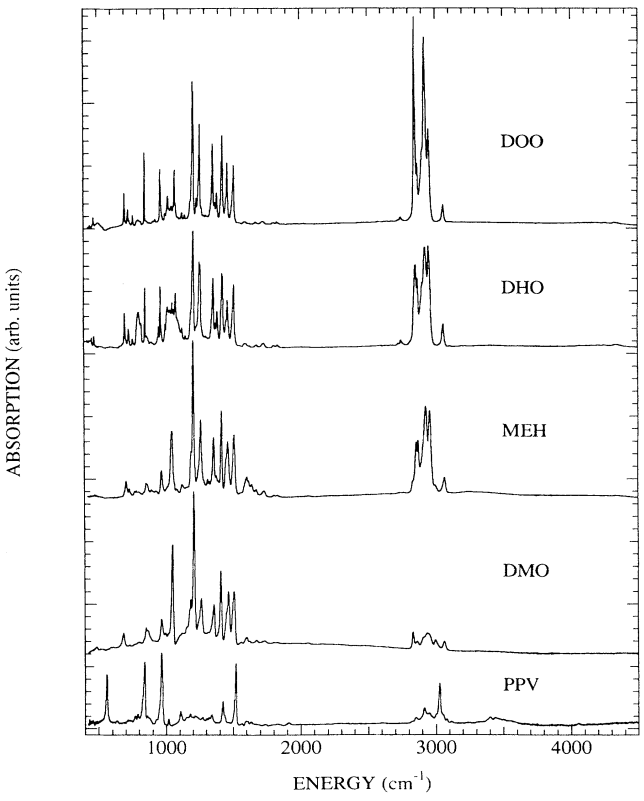

FIG. 2. ir spectra from 400 to 4500 cm^{-1} of PPV and its alkoxy derivatives. The spectra have been normalized to the peak of the ring mode at $\sim$ 1510 cm^{-1}. Note the numerous good group frequencies (refer to Table I).

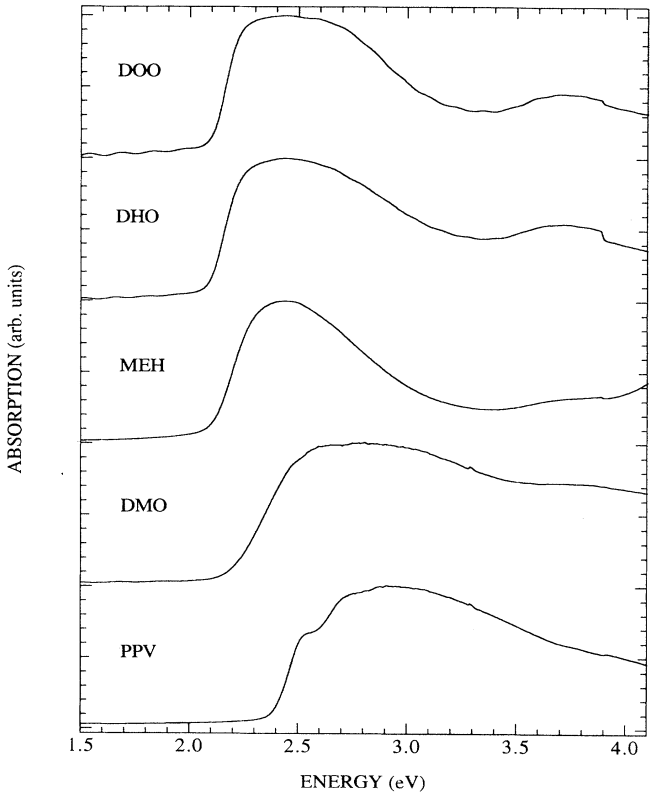

FIG. 3. Near-ir–visible absorption spectra of PPV and its alkoxy derivatives. The spectra have been normalized to the peak of the π-π^* transition. We compute E_{gap} as the intercept between the baseline and the tangent to the absorption edge.

TABLE I. Assignments of the ir-active modes; all the modes were assigned by comparison to group frequencies observed in small molecules (Ref. 18). ϕ refers to the phenylene moiety.

cm^{-1}	PPV	DMO	MEH	DHO	DOO	Expected	Assignment
455	vw					446–485	1-4-ϕ out-of-pl. quadrant bend (Ref. 17)
470		w	w	w	w	~470	1-2-4-5-ϕ out-of-pl. quadrant bend (Ref. 17)
555	s					446–552	1-4-ϕ out-of-plane quadrant bend (Ref. 17)
634	w					615–660	1-4-ϕ in-plane quadrant bend (Ref. 17)
684	w					?	O-CH_3 rock (Ref. 17)
700–704		m	m	m	m	?	O-CH_2 rock (Ref. 17)
714–761	m	vw	w	m	m	720–728	CH_2 rock
781	vw					?	see Ref. 17
784	vw					817	asym. 1-4-ϕ out-of-plane C-H wag
798–823				w	m	790	ϕ ring in-plane quadrant bend
837	s					840	sym. 1-4-ϕ out-of-plane C-H wag
851–857	w	m	m	s	s	860–900	sym. 1-2-4-5-ϕ C-H out-of-plane wag
865		m	m	w	w	864	asym.1-2-4-5-ϕ C-H in-plane wag
873	w					940	sym. 1-4-ϕ out-of-plane C-H wag
881–889	w			w		876	asym.1-2-4-5-ϕ C-H out-of-plane wag
926	w					961	asym. 1-4-ϕ out-of-plane C-H wag
952–966			w	m	m	961	asym. 1-4-ϕ out-of-plane C-Hwag
962–969	s	s	s	s	s	992	ϕ ring breathing
1000–1100				a	b	1000–1100	CH_2 wag band
1072–1077				s	s	~1040	ϕ-alkoxy stretch
1046–1047		s	s			~1040	ϕ-alkoxy stretch
1106	m					1110–1120	1-4-ϕ C-H in-plane bend
1103–1165		vw	w	w	w	?	1-2-4-5-ϕ C-H in-plane bend
1121			w			1151–1159	tertiary C-H wag
1179	vw					?	ϕ C-H in-plane bend
1183–1193		m	w			1169–1181	2,5 vs. 3,6 ring mode
1205–1208		vs	vs	vs	vs	1210	(ϕ-O)-C stretch
1213	vw					?	ϕ C-H in-plane bend
1257		s	s	s	s	1250	ϕ-(O-CH-) stretch
1272	vw					1175–1280	ϕ C-H in-plane bend
1301–1338	c					?	?
1356–1359		s	s	s	s	~1350	-O-CH_3 wag and CH_3 sym. def.
1378			w			1360	tertiary C-H bending
1377–1388	w	w	w	w	w	1350	C-C ring hextant stretch
1389–1390				m	m	1390	-O-CH_2 wag
1406–1423	s	s	s	s	s	1401–1417	C-C ring semi-circular stretch
1452		w	w			1440–1470	(R-O)-CH_3 sym. deformation
1456–1459				w	w	1440–1470	(R-O)-CH_2 sym. deformation
1464–1465				s	s	1450–1475	(R-O)-CH_3 asym. deformation
1465		s	s			1450–1475	(R-O)-CH_2 asym. deformation
1502–1518	1	1	1	1	1	~1510	C-C ring semi-circular stretch
1565	w	w	w	w	w	~1580	C-C quadrant ring stretch
1590–1599	w	w	w	w	w	~1600	C-C quadrant ring stretch
1633–1640	vw		m			1640	*trans*-vinylene C=C stretch
1674–1679		w		w	w	1668–1678	*trans*-vinylene C=C stretch
1730–1735		vw	vw	vw	vw	~1732	overtn: 1-2-4-5-ϕ C-H in-plane wag
1735	vw					?	overtone of ϕ C-H wag
1792	vw					~1780	overtone of ϕ C-H wag
1803			vw	vw	vw	~1814	*trans*-vinylene & ϕ C-H wag
1825	vw					~1806	*trans*-vinylene & ϕ C-H wag
1832–1837		vw	vw	vw	vw	~1827	*trans*-vinylene & ϕ C-H wag
1914	vw			vw	vw	~1926	overtone of *trans*-vinylene C-H wag
2725				vw	vw	~2722	ϕ-(O-CH)$_2$ & ϕ semi-circ.
2744				vw	vw	~2767	ϕ-(O-CH)$_2$ & ϕ semi-circ.
2825–2830	vw	s	w			2835	(RO)-CH_3 overtone
2846–2853	vw	vw	s	s	vs	2845	CH_2 sym. C-H stretch
2859–2867		w	s	s	m	2855	CH_3 sym. C-H stretch
2870			m	m	w	?	CH_2 sym. C-H stretch
2901–2905		m	vw	vw	vw	2908	R-O-CH_3 sym. C-H stretch

TABLE I. (*Continued*).

cm^{-1}	PPV	DMO	MEH	DHO	DOO	expected	assignment
2912	mw					2920	C-H_2 stretch
2921–2926			s	s	s	2916–2936	CH_2 asym. C-H stretch
2953		m				2955–2992	O-CH_3 asym. C-H stretch
2952–2958			s	s	s	2852–2972	CH_3 asym. C-H stretch
2951	w					2950	C-H_2 stretch
2949–2954			s	s	ms	2950–2960	CH_3 asym. C-H stretch
2993–2996		m	mw			2972–2995	O-CH_3 sym. C-H stretch
3002	w					3000–3200	ϕ C-H stretch
3023	s					3000–3050	C-H *trans*-vinylene stretch
3031–3048	w			vw	vw	3000–3200	ϕ C-H stretch
3057–3063		s	s	s	s	3000–3050	C-H *trans*-vinylene stretch
3079	w					3000–3200	ϕ C-H stretch
3106–3112	w	vw	vw	vw	vw	3000–3200	ϕ C-H stretch

[a] 1000, 1017, 1035, 1051, 1060, 1095: band in DHO.
[b] 1003, 1022, 1034, 1049, 1072, 1097: band in DOO.
[c] 1301, 1311, 1228: band in PPV.

troduction of two alkoxy groups of disparate size causes a single ring unit cell to become noncentrosymmetric. Only one of the two sterically preferable head-to-tail configurations (see Fig. 1) can restore inversion symmetry in a doubled unit cell. The strength of the *trans*-vinylene C=C stretch mode in MEH indicates some inversion symmetry breaking in the system.

The optical absorption spectra for PPV and its alkoxy derivatives appear in Fig. 3. We define the energy gap E_{gap} as the onset of the absorption edge, consistent with photoconductivity experiments[19] in these polymers, which show the onset of the photocurrent at those energies. We note that band gap decreases by ~ 0.3 eV with the introduction of alkoxy side chains. The addition of electron-donating oxygen orbitals (two per monomer unit) adjacent to the polymer backbone raise both the highest occupied molecular orbital (HOMO) and the lowest unoccupied molecular orbital (LUMO), but decreases their relative separation.[8,20] While steric effects due to the long side chains could cause conformational defects which disrupt conjugation of the π-electron system and can thus affect the band gap (as, e.g., in thermochromism[21–23]), such defects would increase the π-π^* gap by shortening the effective conjugation length of the polymer chain. Thus, the shift of the π-π^* interband absorption in these systems is due neither to conformational nor steric effects, but rather is electronic in origin.

B. Photoinduced and doping-induced spectroscopy

We present ir photoinduced (PI) absorption spectra of PPV (Ref. 24) and its alkoxy derivatives at 10 K with

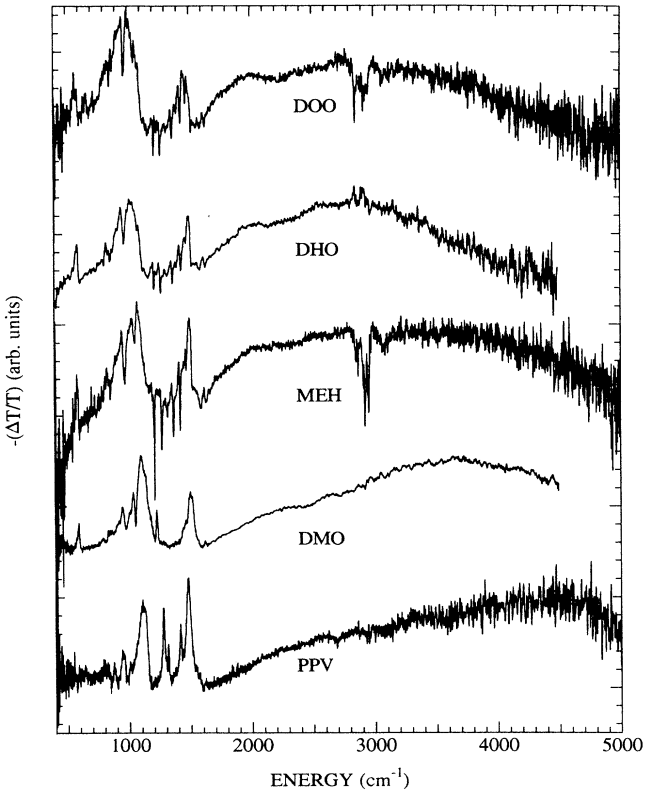

FIG. 4. ir photoinduced absorption spectra of PPV and its alkoxy derivatives. The spectra have been normalized to the peak of the lower bipolaron absorption at ω_-.

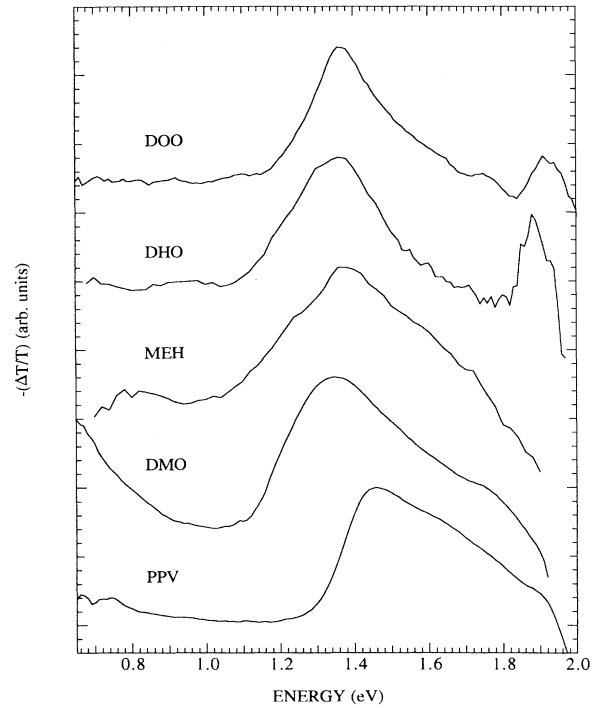

FIG. 5. Near-ir–visible photoinduced spectra of PPV and its alkoxy derivatives. The spectra have been normalized to the peak of the upper bipolaron absorption at ω_+.

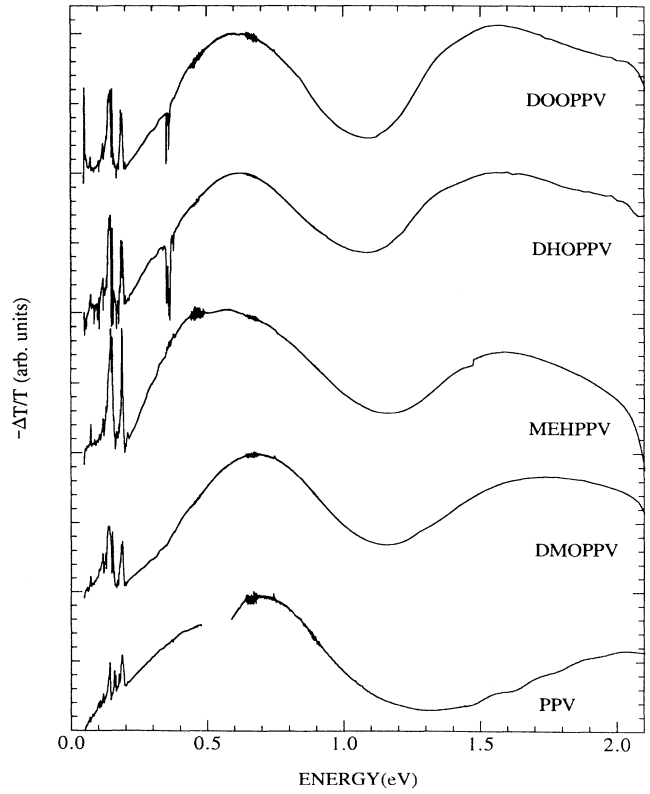

FIG. 6. Doping-induced absorption spectra of PPV and its alkoxy derivatives. We have fit the ir data to match the visible data.

a resolution of 2 cm^{-1} in Fig 4. The data are plotted as $-\Delta T/T$ versus frequency, where T is the transmission and ΔT is the photoinduced change in the transmission. In all the materials, we observe strong PI IRAV modes associated with the translational degrees of freedom of the charged excitations. In addition, we find a broad electronic transition whose peak, at ω_-, red shifts from 0.54 eV in PPV to 0.35 eV in DOO. In Fig. 5 we present the photoinduced absorption spectra of PPV and its alkoxy derivatives at 80 K from the near ir to the visible. The data show a second broad electronic transition whose peak, at ω_+, red shifts from 1.46 eV in PPV to 1.36 eV in DOO. In both Figs. 4 and 5, the spectra have been normalized to the intensity of the peaks at ω_- and ω_+.

Figure 6 presents $\Delta T/T$ of PPV and its alkoxy derivatives upon doping. A direct correspondence between doping-induced (DI) and PI spectral features is clearly evident. The presence of the two subgap electronic absorptions and the development of IRAV modes upon both PI and DI carrier injection suggests that the dominant charged excitation in PPV and its alkoxy derivatives are bipolarons.[1]

IV. DISCUSSION

A. Bipolaron excitations

From the spacing between the two subgap bipolaron absorptions, we can directly extract the confinement parameter given in terms of the quotient ω_0/Δ, where $2\omega_0 = \omega_+ - \omega_-$ is the separation between the two bipolaron levels and $\Delta = E_{gap}/2$ is half the bandgap. In the model of Fesser, Bishop, and Campbell,[25] the confinement parameter γ is defined as

$$\gamma = \frac{(\omega_0/\Delta)\ \arcsin(\omega_0/\Delta)}{\sqrt{1-(\omega_0/\Delta)^2}}. \tag{1}$$

Table II lists the observed peak energies for ω_- and ω_+, while Table III presents our calculated confinement parameters. The measured values of γ are between those established for poly(3-hexyl thiophene) (P3HT; γ=0.4) (Ref. 26) and poly(thienlyene-vinlyene) (PTV; γ=0.1).[27] If we view the confinement parameter as a measure of degree to which the ground-state degeneracy is broken, then, in a simplified picture for pseudopolyenes, the larger the number of adjacent *trans*-carbon units along the backbone, the smaller the confinement parameter. *Trans*-polyacelyene has the smallest confinement parameter (γ=0), and *cis*-polyacelyene the largest (γ=0.5 – 1).[25] In this zeroth approximation, we expect PPV and its alkoxy derivatives to have a γ larger than that of PTV and smaller than that P3HT, consistent with our results.

We observe that γ increases with the length of the substitutional groups. We suggest that this is caused by a systematic decrease in the effective conjugation length due to steric hindrance of increasingly longer side chains disturbing the coplanarity of the rings. This is not in con-

TABLE II. A comparison of the bipolaron peak positions ω_+ and ω_- in the PI and DI spectra.

Polymer	E_{gap}	ω_-^{photo}	ω_+^{photo}	ω_-^{dope}	ω_+^{dope}
PPV	2.38 ± 0.01	0.55 ± 0.03	1.46 ± 0.01	0.70 ± 0.02	2.07 ± 0.02
DMO	2.18 ± 0.01	0.45 ± 0.01	1.35 ± 0.01	0.68 ± 0.02	1.76 ± 0.02
MEH	2.10 ± 0.01	0.43 ± 0.02	1.36 ± 0.01	0.57 ± 0.02	1.59 ± 0.02
DHO	2.08 ± 0.01	0.35 ± 0.01	1.36 ± 0.01	0.61 ± 0.02	1.57 ± 0.02
DOO	2.10 ± 0.01	0.37 ± 0.01	1.36 ± 0.01	0.60 ± 0.02	1.55 ± 0.02

tradiction to the insensitivity of the absorption edge to side-chain length (see Fig. 3), where the dominant factor is the electron density being affected by the oxygen.

If we neglect the Coulomb repulsion between the charges forming the PI bipolarons, we expect $\omega_+ + \omega_- = E_{gap}$. Including the Coulomb interaction, the subgap transitions each red shift by an amount U_b, i.e.,

$$\omega_+^{photo} + \omega_-^{photo} = E_{gap} - 2U_b, \tag{2}$$

where U_b is the difference in energy between the doubly charged initial state and the singly charged final state. Since a polaron is the bound state of a neutral and a charged soliton, while a bipolaron is the bound state of two like-charged solitons, a large U_b favors polaron formation. The small values of U_b relative to the energy gap ($U_b/E_{gap} \sim 0.1$) are consistent with bipolaron formation in all the studied polymers. For doping-induced bipolarons, the Coulomb repulsion energy U_b is diminished by the binding energy of the bipolaron to the dopant counter ions, E_b, due to electronic screening, such that[28]

$$\omega_+^{dope} + \omega_-^{dope} = E_g - 2(U_b - E_b). \tag{3}$$

We list the calculated values of U_b and E_b for PPV and its alkoxy derivatives in Table III. Our data show that E_b decreases significantly with increasing side-chain length, implying weaker binding of the bipolarons along the polymer backbone to the dopant ions, and showing that longer side chains increase the distance between the doping ions and the backbone. Thus, we see steric hindrance affecting the nature of the charge carriers on the polymer backbone. It is interesting to note that, even though the Coulomb energy U_b is repulsive, real space electron pairing (bipolaron formation) resulting from electronic confinement induced by the nondegenerate ground state occurs in these systems.

B. Amplitude mode formalism

Theoretically, the one-to-one correspondence between PI IRAV modes, DI IRAV modes, and Raman-active modes was clearly established by Horovitz[29] in terms of amplitude modes associated with the Peierls gap modulation. All photoinduced or doping-induced IRAV modes are related to Raman-active modes by way of an effective Lagrangian corresponding to the motion of charged excitations along the polymer backbone in the presence of both a local pinning potential and an externally applied field. From the equation of motion of the charged excitations, a phonon response function is derived in terms of the "bare" phonon frequency, the natural linewidth, and the component of the total dimensionless electron-phonon coupling constant of each mode. The correct IRAV or Raman mode frequencies are generated by solving the phonon response function in terms of a pinning parameter which is a reflection of the strength of the pinning of charged excitations associated with defects on the chain.

C. Infrared-active vibrational modes

As a result of amplitude mode formalism, we can associate each IRAV mode directly to one Raman-active mode. In Table IV we list the observed DI and PI IRAV mode frequencies of PPV and compare them to the observed frequencies of Raman-active modes in this

TABLE III. Observed and calculated parameters in the PPV series.

Polymer	Δ	ω_0^{photo}	ω_0^{dope}	ω_0^{photo}/Δ	γ^a	$U_b{}^b$	$E_b{}^c$
PPV	1.19	0.46	0.69	0.38	0.16	0.19	0.38
DMO	1.09	0.45	0.54	0.41	0.19	0.19	0.32
MEH	1.05	0.47	0.51	0.44	0.23	0.16	0.19
DHO	1.04	0.51	0.61	0.49	0.28	0.19	0.24
DOO	1.05	0.50	0.59	0.47	0.26	0.19	0.21

[a]Calculated from Eq. (1).
[b]Calculated from Eq. (2).
[c]Calculated from Eq. (3).

TABLE IV. Infrared-active vibrational modes (IRAV's) in PPV.

Raman (Refs. 30 and 31)	Dope	Photo	Assignment (Ref. 18)
	553	549	ϕ in-plane quadrant deformation
	650	620	?
	811	797	?
	837	820	ϕ in-plane quadrant deformation
	876	872	ϕ in-plane hextant deformation
966	960	947	ϕ C-C asymmetric hextant breathing
1100	1003	1003	ϕ C-C asymmetric hextant breathing
1172	1150	1113	ϕ C-C symmetric hextant stretch
1327	1281	1275	*trans*-vinylene C-C stretch
1409	1314	1318	ϕ C-C symmetric hextant stretch
1547	1419	1414	ϕ C-C symmetric semicircle stretch
1586	1505	1480	ϕ C-C symmetric quadrant stretch
1628	1619	1621	*trans*-vinylene C=C stretch

system.[30,31] For the frequency range in which Raman measurements are available, this correspondence between the IRAV modes and Raman modes of PPV is clearly shown by our data. In addition, we make preliminary assignments of the observed IRAV modes to specific structural vibrations. In Table V we list the measured IRAV mode frequencies for the alkoxy derivatives of PPV and compare them to those of the unsubstituted polymer. Correspondence between the substituted and unsubstituted polymers is reasonable, since systems with identical substitution at the 2,5-phenylene ring carbons retain high symmetry. However, mode assignment in the alkoxy PPV derivatives is difficult due to the signal-to-noise ratio and a strong bleaching of out-of-plane ir modes (see below). Consequently, the assignments of the IRAV modes in the alkoxy derivatives of PPV are only suggested. To understand the lattice dynamics of these systems, a complete amplitude mode formalism analysis would be needed. Such a calculation would require presently unavailable Raman scattering data for the alkoxy derivatives of PPV, and is clearly beyond the scope of the present work. As shown in Fig. 2, the addition of alkoxy side chains does not significantly change the frequencies of the ir-active modes associated with carbon-carbon vibrations of the backbone, indicating that the carbon-carbon force constants are essentially independent of the length of the 2,5 substituents. Therefore, we find it unlikely that the Raman frequencies of the PPV alkoxy derivatives should change significantly from the unsubstituted system, and we will assume that the Raman-active modes for the other systems are the same as observed in PPV.

D. Lattice distortions

Based upon the preliminary mode assignments, we can describe the structural nature of charged excitations in PPV and its alkoxy derivatives. All of the IRAV modes are associated with in-plane motion of carbon atoms, as has been confirmed in studies of oriented samples of these materials.[32] Vibrations involving the phenylene moiety

TABLE V. Infrared-active vibrational modes (IRAV's) of PPV and its alkoxy derivatives (PI/DI).

PPV	DMO	MEH	DHO	DOO
549/553	592/597	583/596	588/596	569/596
620/650	- /649	699/625		666/ -
797/811	- /723	- /707	690/ -	
820/837	788/800	- /793		722/ -
872/876	846/842	823/847	786/ -	- /834
947/960	919/919	900/932	823/ -	840/ -
1003/1003	947/947	947/958	943/958	924/957
1113/1150	1099/1113	1030/1044	1012/ -	994/1020
1275/1281	1124/1136	1072/1123	1040/1130	994/1130
1314/1318	1225/1231	1114/1200	1084/1190	1055/1190
1414/1419	1449/1486	1440/1466	1433/1455	1418/1440
1480/1505	1500/1519	1496/1516	1496/1510	1460/1505
1621/1619	1618/1618	1616/1623	1616/1617	1613/1616
- /1682		- /1685	- /1685	- /1690

are numerous, and both the *trans*-vinylene C=C and C-C stretch modes are observed. It is clear that the phenylene moiety in PPV and its alkoxy derivatives retains a strong aromatic character. This is in contrast to the case of PT, where the involvement of thiophene heteroatom in the electronic system is sufficiently weak to characterize the system as a pseudopolyene.[28] In addition, significant phenylene ring deformation associated with the motion of charged excitations is evident, with the degree of ring deformation increasing with increasing sidechain length.

In Fig. 4 we also observe a series of well-defined photoinduced and doping-induced bleaching at ~ 700, ~ 840, ~ 970, ~ 1207, ~ 1263, ~ 1357, ~ 1430, and in the ~ 3000-cm^{-1} region. These bleaches can be traced to out-of-plane ir absorptions (see Table I) involving the C-H wag on the phenylene and *trans*-vinylene moiety, the C-O stretch and wag, the C-C phenylene semicircle stretch, and the C-H stretch region on the alkoxy groups. Thus, they can be understood as a weak heating signature. In studies on oriented samples,[32] these bleachings decouple from the in-plane IRAV modes and allow clear identification of the IRAV spectra.

In the PI absorption spectra, we note the appearance of two overtone peaks at ω_l and ω_h, respectively, as additional structure on top of the lower bipolaron peak in the region of 2000–3000 cm^{-1}. A calculation of the polaron absorption spectrum using the Holstein model[33] predicts the presence of overtone bands. To our knowledge, such overtone bands have not previously been identified in the context of bipolarons in conducting polymers. The large width of the overtone bands suggests that the modes from which they are derived could have significant dispersion. Unfortunately, this large width and the low intensity of the overtone absorptions hinders an unambiguous assignment of the modes. However, we propose assignment of the lower frequency mode to an overtone mode of the *trans*-vinylene C-C stretch mode and assignment of the higher frequency mode to a combination band of the *trans*-vinylene C-C stretch mode with the phenelyene C-C symmetric quadrant stretch mode. In Table VI we list the overtone modes, calculate the proposed underlying frequencies, and compare them with the specific IRAV mode frequencies for the various polymers. Based on this assignment, we conclude that the *trans*-vinylene C-C stretch mode observed at 1275 cm^{-1} in PPV red shifts to 1124 cm^{-1} in DMO, to 1078 cm^{-1} in MEH, to 1040 cm^{-1} in DHO, and to 994 cm^{-1} in DOO. This assignment enables us to conclude that these IRAV modes couple strongly to the photoinjected carriers.

TABLE VI. Comparison of the photoexcited overtone spectra and the assignment of the IRAV.

Polymer	ω_l	ω_h	$\frac{\omega_l}{2}$	C-C[a]	$\omega_h - \frac{\omega_l}{2}$	ϕ[b]
PPV	2600	2850	1300	1275	1550	1480
DMO	2300	2650	1150	1124	1500	1500
MEH	2000	2500	1000	1072	1500	1496
DHO	2000	2540	1000	1040	1500	1496
DOO	1970	2500	985	990	1515	1460

[a] *trans*-vinylene C-C stretch mode.
[b] ϕ C-C symmetric quadrant stretch.

E. Pinning of the bipolarons

From trends observed in the IRAV modes, we can make qualitative statements regarding pinning and confinement in these systems even without a direct amplitude mode formalism fit.

We expect the frequency of the IRAV modes to be red shifted from those of the corresponding Raman modes. Specifically, the size of the red shift for any given mode is dependent upon the size of the electron-phonon coupling constant and the pinning strength in the given system: the weaker the pinning for a given system or the stronger a given mode is coupled, the greater the the magnitude of red shift. As shown in Table V, the red shift of the IRAV modes grows dramatically with increasing side-chain length. In particular, the red shift of the PI *trans*-vinylene C-C stretch IRAV mode grows from ~ 46 cm^{-1} in PPV to ~ 333 cm^{-1} in DOO. In comparing PPV and its alkoxy derivatives, it is reasonable to assume that the electron-phonon coupling strengths of the backbone carbon-carbon modes should be mostly insensitive to the addition of side chain, implying that the pinning strength of bipolarons decreases with increasing side-chain length.

When we compare the frequencies of the Raman modes, the PI IRAV modes, and the DI IRAV modes in PPV and its alkoxy derivatives, we see that the PI modes are red shifted with respect to the DI modes, which, in turn, are red shifted with respect to the Raman modes. We expect strong pinning of DI excitations due to Coulomb binding of bipolarons to dopant counter ions, and weak pinning of PI excitations, where no counter ions are present. Therefore, the magnitude of the red shift of DI IRAV frequencies should be smaller than that for PI IRAV modes. Indeed, for a perfect system, the pinning of PI charges should be negligible reflecting mainly intrinsic pinning mechanisms, and the lowest-energy IRAV mode should go to zero frequency due to translation invariance. For PPV, the shift of the *trans*-vinylene C-C stretch mode from DI to PI is only ~ 6 cm^{-1}, and the shift of the DI mode from the Raman frequency is only ~ 46 cm^{-1}. In contrast, the shifts for DOO are ~ 136 and ~ 333 cm^{-1}, respectively. We conclude that the magnitude of the red shift between PI and DI modes increases with length of the side chain, and that the pinning of PI bipolarons in PPV is considerable, whereas the pinning is weaker for the alkoxy derivatives. One possible mechanism for these systematic changes in the intrinsic pinning in these systems is Coulomb binding between bipolarons on adjacent chains. If this were true, the reduction of interchain coupling due to the steric hindrance of the side chains would explain the relatively weak pinning of photoinduced bipolarons in the alkoxy PPV derivatives.

V. CONCLUSION

We have characterized the vibrational and electronic structure of both the ground state and excited states of the conjugated polymer poly(1,4-phenylene-vinylene) (PPV) and a series of its alkoxy derivatives including poly(2,5-methoxy-PV) (DMO), poly(2,5-hexoxy-PV) (DHO), poly(2,5-octoxy-PV) (DOO), and poly[2-methoxy,5-(2′ ethyl-hexoxy)-PV] (MEH). We have demonstrated that the charged excitations in these systems are spectroscopically consistent with bipolarons. The measured red shifts of the IRAV mode frequencies in the alkoxy derivatives of PPV indicate that the pinning strength of bipolarons decreases as the length of the side chain increases. We determine that the confinement parameter γ increases while the Coulomb interaction energy U_b remains unchanged and the Coulomb binding energy E_b decreases with increasing side-chain length.

ACKNOWLEDGMENTS

We wish to acknowledge fruitful discussions with J.-L. Brédas and T. W. Hagler. We would also like to thank S. Phillips, D. Spiegel, M. Nowak, and Y.-H. Kim for their help. This work was supported by ONR Grant No. N-000-14-83-K-0450.

[1] For a review, see, e.g., A. J. Heeger, S. Kivelson, J. R. Schrieffer, and W. P. Wu, Rev Mod. Phys. **60**, 781 (1988) .
[2] S. A. Brazovskiĭ and N. N. Kirova, Pis'ma Zh. Eksp. Teor. Fiz. **33**, 6 (1981) [JETP Lett. **33**, 4 (1981)].
[3] D. McBranch, M. Sinclair, A. J. Heeger, A. O. Patil, S. Shi, S. Askari, and F. Wudl, Synth. Metals **29**, E85 (1989).
[4] I. Murase, T. Ohnishi, T. Naguchi, and M. Hirooka, Polym. Comm. **25**, 327 (1984).
[5] D. D. C. Bradley, J. Phys. D **20**, 1389 (1987).
[6] D. D. C. Bradley, R. H. Friend, H. Lindenberger, and S. Roth, Polymer **27**, 1709 (1986).
[7] D. D. C. Bradley, G. P. Evans, and R. H. Friend, Synth. Metals **17**, 651 (1987).
[8] H. Eckhardt, L. W. Shacklette, K. Y. Jen, and R. L. Elsenbaumer, J. Chem. Phys. **91**, 1303 (1989).
[9] H. Bleier, Y. Q. Shen, D. D. C. Bradley, H. Lindenberger, and S. Roth, Synth. Metals **29**, E73 (1989).
[10] S. H. Askari, S.D.D.V. Rughooputh, F. Wudl, and A. J. Heeger, Polym. Mater. Sci. Eng. **59**, 123 (1988).
[11] F. Wudl, P.-M. Allemand, G. Srdanov, Z. Ni and D. McBranch, ACS Symp. Ser. **455** (1991).
[12] I. Murase T. Ohnishi, T. Noguchi, and M. Hirooka, Synth. Metals **17**, 639 (1987).
[13] R. A. Wessling, R. G. Zimmerman, U.S. Patent Nos. 3,401,152 (1968), 3,404,132 (1968), 3,532,643 (1970), 3,705,677 (1972); R. A. Wessling, J. Polym. Chem. Polym. Symp. **72**, 55 (1985).
[14] T. Mommi, S. Tokito, T. Tsustui, and S. Saito, Chem. Lett. **7**, 1201 (1988).
[15] K.-Y. Jen, L. W. Shacklette, and R. Elsenbaumer, Synth. Metals **22**, 179 (1987).
[16] B. G. Blanchet, C. R. Fincher, T.-C.Chung, and A. J. Heeger, Phys. Rev. Lett. **50**, 1939 (1983).
[17] L. A. Gribov, I. E. Davidova, R. Kostić, and D. Raković, J. Mol. Struct. **216**, 214 (1990).
[18] (a) N. B. Colthup, L. H. Daly, and S. E. Wiberley, *Introduction to Infrared and Raman Spectroscopy* (Academic, New York, 1975); (b) L. J. Bellamy, *The Infra-red Spectra of Complex Molecules* (Chapman and Hall, London, 1975), and references therein; (c) D. H. Williams and I. Fleming, *Spectroscopic Methods in Organic Chemistry* (McGraw-Hill, London, 1980); (d) H. P. Latscha and H. A. Klein, *Organische Chemie (Heidelberger Taschenbücher)* (Springer-Verlag, Berlin, 1982); (e) C. N. R. Rao, *Chemical Applications of Infrared Spectroscopy* (Academic, New York, 1963); (f) N. L. Alpert, W. E. Keiser, and H. A. Szymanski, *IR Theory and Practice of Infrared Spectroscopy* (Plenum, New York, 1970); (g) S. E. Wiberley, S. C. Bunce, and W. H. Bauer, Anal. Chem. **32**, 217 (1960).
[19] G. Yu (private communication).
[20] J.-L. Brédas (private communication).
[21] O. Inganäs, G. Gustafsson, and W. R. Salanek, Synth. Metals **28**, C377 (1989).
[22] K. Yoshimo, S. Nakahma, S. B. Gu, and R. Sugimoto, Jpn. J. Appl. Phys. **26**, L2046 (1987).
[23] B. Thémans, W. R. Salanek, and J.-L. Brédas, Synth. Metals **28**, C359 (1989).
[24] D. D. C. Bradley, R. H. Friend, R. H. Pratt, F. L. Wong, K. S. Hayes, W. Lindenberger, and S. Roth, *Proceedings af an International Winter School in Kirchberg, Tirol*, 1987, edited by H. Kuzmany, M. Mehring, and S. Roth, Springer Series in Solid-State Sciences Vol. 76 (Springer-Verlag, Berlin, 1987).
[25] K. Fesser, A. R. Bishop, and D. K. Campbell, Phys. Rev. B **27**, 4804 (1983).
[26] Y. H. Kim, D. Spiegel, S. Hotta, and A. J. Heeger, Phys. Rev. B **38**, 5490 (1988).
[27] A. J. Brasset, N. F. Colaneri, D. D. C. Bradley, R. A. Lawrence, R. H. Friend, H. Murata, S. Tokito, T. Tsutsui, and S. Saito, Phys. Rev. B **41**, 10586 (1990).
[28] Z. Vardeny, E. Ehrenfreund, O. Brafman, M. Nowak, H. Schaffer, A. J. Heeger, and F. Wudl, Phys. Rev. Lett. **56**, 671 (1986).
[29] B. Horovitz, Solid State Commun. **41**, 729 (1982).
[30] S. Lefrant, E. Perrin, J. P. Buisson, H. Eckardt, and C. C. Han, Synth. Metals **29**, E91 (1989).
[31] Y. Furukawa, A. Sakamoto, and M. Tasumi, J. Chem. Phys. **93**, 5354 (1989).
[32] L. Smilowitz, C. M. Foster, K. F. Voss, and A. J. Heeger (unpublished).
[33] H. G. Reik and R. Mühlstroh, Solid States Commun. **5**, 105 (1967).